

Spin Wave Propagation through Antiferromagnet/Ferromagnet Interface

Oksana Busel,^{1,2,*} Oksana Gorobets,² and Oleg A. Tretiakov^{3,†}

¹Nano and Molecular Systems Research Unit, University of Oulu, Oulu 90014, Finland

²Faculty of Physics and Mathematics, National Technical University of

Ukraine “Igor Sikorsky Kyiv Polytechnic Institute,” Kyiv 03056, Ukraine

³School of Physics, The University of New South Wales, Sydney 2052, Australia

(Dated: December 29, 2021)

We study the problem of controlling spin waves propagation through an antiferromagnet/ferromagnet interface via tuning material parameters. It is done by introducing the degree of sublattice noncompensation of antiferromagnet (DSNA), which is a physical characteristic of finite-thickness interfaces. The DSNA value can be varied by designing interfaces with a particular disorder or curvilinear geometry. We describe a spin-wave propagation through any designed antiferromagnet/ferromagnet interface considering a variable DSNA and appropriate boundary conditions. As a result, we calculate the physical transmittance and reflectance of the spin waves as a function of frequency and show how to control them via the exchange parameters tuning.

Antiferromagnets (AFMs) are attractive as active elements for next-generation spintronic devices [1–4]. The disadvantage of the last generation of spin-wave (SW) devices is their relatively low operating frequency, which is limited by the GHz range [5–9]. However, recent trends involving AFMs allow to raise this frequency to THz to successfully compete with optical devices [10–13], because a spin manipulation in AFMs is inherently faster than in ferromagnets (FM) [14, 15]. The ultrafast generation, detection, and gate tuning of spin waves in AFMs are now becoming more and more accessible [15, 16], meanwhile the detection techniques in FMs are still better established [17–19].

The benefits of using AFMs have been recently actively studied [20–28]. Usually, AFMs are considered in limiting cases, namely, compensated, when the AFM has no static magnetization at the interface [29], and noncompensated, when the boundary of the AFM is magnetized [30]. AFMs with the fully compensated spin moments have implementations in terahertz range [31–33], e.g., spin-current driven AFM nano-oscillators have been proposed [34, 35]. On the other hand, the mechanisms of the AFM domain switching by current pulses [36–38] in certain cases are based on the electric field or spin torques acting on the noncompensated spins at the AFM interface [39, 40]. However, in some problems such as transmission of the spin current through a thin AFM insulator by means of evanescent AFM SWs, it has been recently assumed that the AFM could be partially noncompensated at the interface [41]. Moreover, it has been pointed out that the effective magnetic moment can be a complex arrangement of not fully compensated moments along compensated AFM structures [42]. Considering the compensated or noncompensated limiting cases significantly simplifies the description of underlying AFM physics, but does not cover the entire spectrum of the AFMs, and furthermore, requires perfectly flat AFM interfaces. Meanwhile, realistic rough interfaces with a variable degree of sublattice noncompensation are more common and therefore important to study.

In this paper, we investigate the SWs propagation through AFM/FM interface of a complex geometry. This problem can be solved by introducing an averaged characteristic of

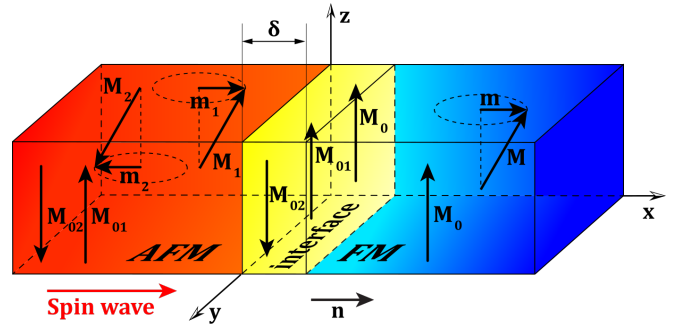


FIG. 1. A schematic representation of two-sublattice AFM, the interface of finite thickness between AFM and FM, FM and magnetizations in each layer.

this interface – degree of sublattice noncompensation of AFM (DSNA). Due to strong exchange interactions between the AFM sublattices and with a neighboring material, this concept may play a crucial role in describing complex AFM interfaces with other magnetic media, i.e., those with a specific disorder or of curvilinear geometry. Complex interfaces with variable DSNA can be manufactured in a variety of ways, such as by engineering a particular surface roughness, ion implantation, vapor deposition or introduction of other defects [43–47].

We develop an analytical approach to a SW propagation from AFM to FM through any designed AFM/FM interface described by a variable DSNA. We consider the scattering of exchange SWs at the AFM/FM interface of finite thickness sandwiched between AFM and FM. We obtain the complete relations between the phases and amplitudes of scattered SWs taking into account the Poynting vector continuity at the boundary. This theory is designed for an exchange dominated regime, in which we derive the interface boundary conditions in the vicinity of noncompensated case, i.e., the DSNA $\mu \rightarrow 0$. This case is of high interest as it gives rise to the largest exchange bias in AFM/FM structures. As a result, the frequency dependences of SW transmittance and reflectance at the interface are found in $\mu \rightarrow 0$ case.

Model. We consider a one-dimensional scenario of SW

propagation through an AFM/FM interface (along the x -axis) as shown in Fig. 1. The interface has thickness δ and is parallel to the y - z plane. Since AFM has two sublattices and FM has one, we introduce three static (ground state) magnetizations within the interface and its surroundings, \mathbf{M}_{01} , \mathbf{M}_{02} , and \mathbf{M}_0 , respectively. The media are magnetized by a strong enough uniform external magnetic field along the z -axis, so all ground state magnetizations are (anti)parallel to the z -axis. The small deviations of the magnetizations $\mathbf{M}_{1(2)}$ and \mathbf{M} from the ground state are introduced in the form $\mathbf{M}_{1(2)} = \mathbf{M}_{01(02)} + \mathbf{m}_{1(2)}$ and $\mathbf{M} = \mathbf{M}_0 + \mathbf{m}$, where $\mathbf{m}_{1(2)}$ and \mathbf{m} are the dynamical components of the magnetization for the two AFM sublattices and FM, respectively, i.e., $m_{1(2)} \ll M_{01(02)}$ and $m \ll M_0$.

To present the analytical theory of the SW propagation through the AFM/FM interface in an exchange dominated regime, only the exchange interactions between AFM and FM have to be taken into account within the interface [48–50]. We describe the magnetization dynamics by the Landau-Lifshitz (LL) equation [51], $\partial \mathbf{M}_l / \partial t = \gamma \mathbf{M}_l \times \mathbf{H}_l^{\text{eff}}$, where γ is the gyromagnetic ratio and $\mathbf{H}_l^{\text{eff}} = -\delta W_l / \delta \mathbf{M}_l$ is the effective magnetic field in each material. Here W_l is the interfacial magnetic energy, and labels l represent the two AFM sublattices and the one of FM. Integrating over the interface one finds the energy $W_i = S \int_0^\delta w_i dx$ with S being the cross-sectional area and the energy density at the interface w_i :

$$w_i = A(x) \mathbf{M}_1 \mathbf{M}_2 + A_1(x) \mathbf{M}_1 \mathbf{M} + A_2(x) \mathbf{M}_2 \mathbf{M} + \frac{\alpha(x)}{2} \left(\frac{\partial \mathbf{M}}{\partial x} \right)^2 + \frac{\alpha_1(x)}{2} \left[\left(\frac{\partial \mathbf{M}_1}{\partial x} \right)^2 + \left(\frac{\partial \mathbf{M}_2}{\partial x} \right)^2 \right] + \alpha_2(x) \frac{\partial \mathbf{M}_1}{\partial x} \frac{\partial \mathbf{M}_2}{\partial x}. \quad (1)$$

Here $A(x)$ is the homogeneous AFM exchange parameter, $A_{1(2)}(x)$ is the exchange coupling parameter of each AFM sublattice with the FM, $\alpha = \alpha_{\text{ex}} / M_0^2$ is the inhomogeneous FM exchange parameter, α_1 is the inhomogeneous exchange self-interaction parameter for each AFM sublattice, and α_2 is the inhomogeneous exchange interaction parameter between the AFM sublattices ($\alpha_n = \alpha_{\text{ex},n} / M_{0n}^2$ with $n = 1, 2$ and $\alpha_{\text{ex},n}$ being the exchange stiffness constants [52]). Parameter A can be estimated by $A \sim \alpha_{\text{ex},1} / (M_{01(02)}^2 d^2)$, where d is the lattice constant of the AFM [52–54]. The interactions in Eq. (1) include the antiferromagnetic coupling between two sublattices, the two couplings between each AFM sublattice and the FM [31], the exchange stiffness interaction of FM, the exchange self-interaction of the AFM sublattices, and the exchange interaction between AFM sublattices, respectively.

AFM/FM boundary conditions. To derive the interfacial boundary conditions, order parameters \mathbf{M}_1 , \mathbf{M}_2 and \mathbf{M} are considered as slowly varying functions, whereas the coefficients $A_1(x)$, $A_2(x)$, $A(x)$, $\alpha_1(x)$, $\alpha_2(x)$, and $\alpha(x)$ are varying significantly within the interface $[0, \delta]$ as shown in Fig. 2 (a). We define the interface in terms of the averaged properties of the surrounding materials, so the LL equations are integrated over the thickness δ of the interface [48, 55–57]. Then at the interface, the solutions of the LL equations satisfy the bound-

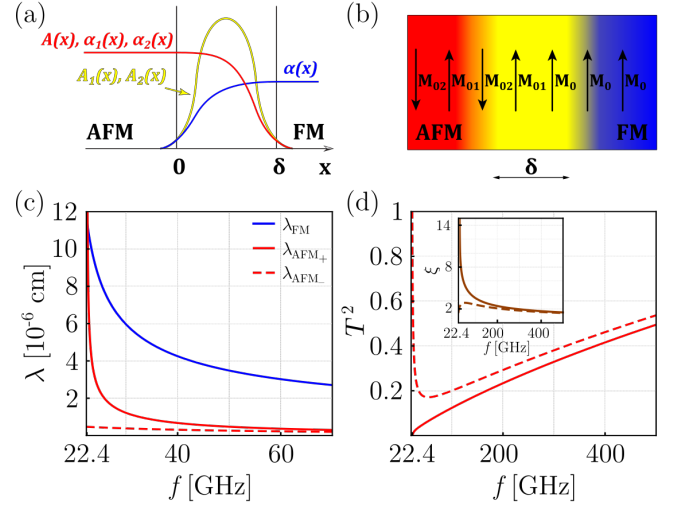


FIG. 2. (a) Schematic spatial dependence of all material parameters characterizing AFM/FM interface, Eq. (1). (b) One-dimensional model for noncompensated AFM at the AFM/FM interface. (c) The dependence of the SW wavelength λ and (d) normalized transmittance T^2 on frequency f . In (c), the solid blue curve represents the FM branch, while in (c) and (d) the solid and dashed red curves correspond to the plus and minus AFM branches, respectively. In (d), $T^2(f)$ is given according to Eq. (9) without the influence of the additional factor ξ . The inset in (d) illustrates $\xi(f)$, according to Eq. (12).

ary conditions:

$$A_1 m + \left(A - \nu A_1 - \alpha_1 \frac{\partial}{\partial x} \right) m_1 + \left(A - \alpha_2 \frac{\partial}{\partial x} \right) m_2 = 0, \quad (2a)$$

$$A_2 m + \left(A + \nu A_2 - \alpha_1 \frac{\partial}{\partial x} \right) m_2 + \left(A - \alpha_2 \frac{\partial}{\partial x} \right) m_1 = 0, \quad (2b)$$

$$\left(A_1 - A_2 - \nu \alpha \frac{\partial}{\partial x} \right) m - \nu A_1 m_1 - \nu A_2 m_2 = 0, \quad (2c)$$

for the dynamical magnetization components in FM, $\mathbf{m} = (m_x, m_y, 0)$, and AFM, $\mathbf{m}_{1(2)} = (m_{1(2),x}, m_{1(2),y}, 0)$. For convenience we expressed them via the cyclic variables $m_{1(2)} = m_{1(2),x} + i m_{1(2),y}$ and $m = m_x + i m_y$. We also used $M_{02}/M_{01} = 1$ for the AFM and introduced the notation $M_0/M_{01} = \nu$. Eqs. (2) represent the set of linearized boundary conditions for the dynamical magnetization components. Note, that here we have extended the approach of finding boundary conditions for an FM/FM interface [48]. Thus, in our case of the AFM/FM interface, the approach works when the absolute values of the magnetization are approximately equal, i.e. $\nu \approx 1$, and the magnetization of the AFM sublattice closest to the FM boundary is parallel to the FM magnetization, see Fig. 2 (b), that is called noncompensated AFM boundary case. Since the AFM dynamical magnetization components are strongly coupled, the contribution from both AFM sublattices is effectively included in the interface, but boundary conditions (2) are greatly simplified.

To obtain the ratio of the AFM dynamical components $\mathbf{m}_2/\mathbf{m}_1$, we solve the set of linearized LL equations for both sublattices [58] and take $M_{01,z} = M$ and $M_{02,z} = -M$, then this

ratio takes the form

$$\sigma(\omega) = -\frac{m_2}{m_1} = \frac{(\Omega_+ + \Omega_-)\omega - \Omega_+\Omega_- - \omega^2}{\Omega_-^2 - \omega^2}, \quad (3)$$

where $\Omega_{\pm} = \gamma M[(\alpha_1 - \alpha_2)k_{AFM}^2 \pm H_e/M + \beta_1 - \beta_2]$, H_e is the external magnetic field, k_{AFM} is the AFM wavevector, β_1 and β_2 are the AFM anisotropy constants, and $\omega = 2\pi f$ with frequency f . Note that for a nonzero magnetic field (along z -axis), the AFM magnetic moments are oriented almost perpendicular to the magnetic field with a slight misalignment along the magnetic field. Thus, in the ground state a small uncompensated magnetic moment would be parallel to the field, while the Néel vector would be perpendicular to it. Therefore, to obtain the desired AFM orientation of Fig. 2 (b), it is known that a strong enough additional easy-axis anisotropy along z -axis has to be included.

DSNA. Using σ from Eq. (3), the linearized boundary conditions (2) can be simplified [59]. The set of these equations has a solution with a nonzero amplitude of the transmitted SW only if the following relations are satisfied: $\mu(\alpha_1 - \alpha_2\sigma) = \alpha_2 - \alpha_1\sigma$, $\mu[A(1 - \sigma) - A_1\nu] = A(1 - \sigma) - A_2\sigma\nu$, and $\mu A_1 = A_2$ with $\mu \neq 0$. Otherwise, the SWs are fully reflected. Thus, we introduce the DSNA μ as

$$\mu = \frac{\alpha_2 - \alpha_1\sigma}{\alpha_1 - \alpha_2\sigma}. \quad (4)$$

Then the coupling parameters between each AFM sublattice and FM, $A_{1(2)}$, are defined through the one between the AFM sublattices, A , and the DSNA μ as

$$A_1(\mu) = \frac{A(\mu - 1)}{\mu\nu}, \quad A_2(\mu) = \mu A_1(\mu), \quad (5)$$

when $\sigma \neq 1$. Note that Eq. (3) is applicable anywhere in the AFM, whereas Eq. (4) is applicable only at the AFM/FM interface. For the noncompensated AFM boundary case we discussed above, Eqs. (4) and (5) imply that $|A_1| \gg |A| \sim |A_2|$ and $\mu \rightarrow 0$.

To derive the boundary conditions for any designed boundary depending on the DSNA, we should take into account in Eqs. (2) the relation between AFM dynamical components [Eq. (3)] and $A_{1,2}(\mu)$ from Eq. (5). This significantly simplifies Eqs. (2):

$$A(1 - \mu)m - \nu \left[A(1 - \sigma\mu) - \mu(\alpha_1 - \alpha_2\sigma) \frac{\partial}{\partial y} \right] m_1 = 0, \quad (6a)$$

$$\left[A(1 - \mu)^2 + \nu^2\mu\alpha \frac{\partial}{\partial y} \right] m - \nu A(1 - \mu)(1 - \sigma\mu)m_1 = 0. \quad (6b)$$

These improved boundary conditions include only one dynamical AFM component, however preserve the information of both AFM sublattices. They are defined for any AFM/FM interface depending on DSNA μ . Thus, when the DSNA is varied, in fact, it changes the ratio of considered spins from the first and second AFM sublattices within the interface.

SW propagation. Next, we consider transmission of SWs from AFM to FM. In this paper we assume the geometric optics approximation for the SWs, since the typical SW wavelengths λ_{sw} in AFM and FM are much larger than the width of the interface, $\lambda_{sw} \gg \delta \sim d$. We look for a solution where the incident and reflected circularly polarized SWs in the AFM and transmitted SW in the FM are monochromatic plane waves $\mathbf{m}(\mathbf{r}, t) = \mathbf{m}(\mathbf{r}) e^{i\omega t}$ with the dynamical components of the magnetization defined as

$$m = \tilde{t} e^{ik_{FM,x}x}, \quad m_{1(2)} = \tilde{I}_{1(2)} e^{ik_{AFM,x}x} + \tilde{r}_{1(2)} e^{-ik_{AFM,x}x}. \quad (7)$$

Here k_{FM} is the FM wavevector, $\tilde{I}_{1(2)}$ is the amplitude of the wave incident onto the first (second) AFM sublattice, $\tilde{r}_{1(2)} = \tilde{R}_{1(2)} e^{i\varphi_{1(2)}}$ and $\tilde{t} = \tilde{T} e^{i\varphi}$ are the complex amplitudes of the reflected wave from first (second) AFM sublattice and transmitted wave into the FM, respectively, where $\tilde{R}_{1(2)}$ and \tilde{T} are the real amplitudes, while $\varphi_{1(2)}$ and φ are the phase shifts. Since the problem is formulated in a stationary state, the explicit dependence on time can be neglected here.

Using Eq. (3) the relations between the amplitudes and phase shifts of the AFM sublattices take the form $\tilde{I}_2 = -\sigma\tilde{I}_1$, $\tilde{R}_2 = -\sigma\tilde{R}_1$, and $\varphi_1 = \varphi_2$, respectively. In the following it is convenient to introduce dimensionless complex amplitudes $r_1 = \tilde{r}_1/\tilde{I}_1$ and $t = \tilde{t}/\tilde{I}_1$, then using boundary conditions (6) and expressing $\sigma(\mu)$ from Eq. (4), we obtain $r_1(\mu)$ and $t(\mu)$ shown in [60]. Note that for small $\mu \neq 0$, one can probe different degree of noncompensation by varying μ , while at $\mu \rightarrow 0$ we approach a fully noncompensated AFM boundary case, where our approximation works the best [61]. In this limit the amplitudes take the form

$$r_1 = -\frac{Av^2\alpha\alpha_1k_{FM} - A(\alpha_1^2 - \alpha_2^2)k_{AFM}}{Av^2\alpha\alpha_1k_{FM} + A(\alpha_1^2 - \alpha_2^2)k_{AFM}}, \quad (8)$$

$$t = \frac{2Av(\alpha_1^2 - \alpha_2^2)k_{AFM}}{Av^2\alpha\alpha_1k_{FM} + A(\alpha_1^2 - \alpha_2^2)k_{AFM}}. \quad (9)$$

Thus, to obtain dimensionless reflectance R_1^2 and transmittance T^2 one has to find $|r_1|^2$ and $|t|^2$, respectively.

To determine the spectrum of SWs in AFM and FM we employ well-known dispersion relations for AFM and FM (we consider the case when AFM and FM have anisotropy of the easy-axis type, i.e., $\beta > 0$, $\beta_1 - \beta_2 > 0$, and the total magnetization in AFM is small) [62], respectively:

$$\omega_{\pm}(\mathbf{k}_{AFM}) = \gamma \left(\sqrt{2ak_{AFM}^2 + H_a^2} \pm H_e \right), \quad (10)$$

$$\omega(\mathbf{k}_{FM}) = \gamma \left(2\alpha M_0 k_{FM}^2 + M_0\beta + H_e \right), \quad (11)$$

where $a = A(\alpha_1 - \alpha_2)M^2$, $H_a = M\sqrt{2A(\beta_1 - \beta_2)}$ is the anisotropy field of AFM, $\beta = K/M_0^2$ is the anisotropy constant of FM, and $\omega = 2\pi f$ with frequency f . The AFM has two (plus and minus) dispersion branches, ω_{\pm} . Here we used the dispersion relations for the case of normal incidence of the SW on the AFM/FM interface, the general case of any angle between the SW direction and the interface normal is considered in [59]. According to Eq. (10), to have propagating SWs

in the AFM one has to apply a frequency above $\gamma(H_a \pm H_e)/2\pi$. To activate both AFM branches one has to apply a frequency above $f_a = \gamma(H_a + H_e)/2\pi$.

Assuming that the energy is conserved at the AFM/FM interface [63], the normal component of the energy flux density vector should be continuous at this boundary. In the problem of an interface of two FMs [48], the number of variables that have to be matched at the boundary is the same on both sides, since the FMs have only one magnetization sublattice. Then equating the normal components of the Poynting vectors of both FMs, the sum of the transmittance T^2 and reflectance R^2 at the boundary is $T^2 + R^2 = 1$. However, for an AFM/FM interface, the number of variables to the right and left of the boundary is different, since the AFM has two sublattices (while the FM has only one), see Fig. 2 (b). In this case, one needs to consider the Poynting vector contributions from both AFM sublattices, which significantly complicates the problem. Thus, for the AFM/FM interface, equating the normal components of the Poynting vector of each medium, introduces the factor ξ responsible for the energy conservation at the interface as [64]:

$$R_1^2 + \xi T^2 = 1, \quad \xi = \frac{\alpha k_{FM}}{k_{AFM}[\alpha_1(1 + \sigma^2) - 2\alpha_2\sigma]}. \quad (12)$$

Noting that at the boundary the ratio σ depends on the DSNA μ according to Eq. (4), $\xi(\mu)$ takes the form shown in [65], which in the most relevant fully noncompensated case ($\mu = 0$) gives $\xi = \alpha\alpha_1 k_{FM}/[(\alpha_1^2 - \alpha_2^2)k_{AFM}]$.

To understand the transmittance behavior, we consider its dependence on various magnetic parameters. We take the parameters for a typical AFM/FM interface such as NiO/CoFeB: $M = 0.84$ kG, $M_0 = 1.2$ kG, $\alpha_{ex,1} = 2.8 \times 10^{-8}$ erg/cm, $\alpha_{ex} = 2 \times 10^{-6}$ erg/cm, $d = 4.2 \times 10^{-8}$ cm [66], $H_e = 5$ kOe, $H_a = 3$ kOe, $K = 2.4 \times 10^6$ erg/cm³. To define the proper frequency range for the SWs propagating in the AFM/FM system we determine the reasonable SW wavelengths of AFM $\lambda_{AFM\pm} = 2\pi/k_{AFM}$ and FM $\lambda_{FM} = 2\pi/k_{FM}$ by matching the frequencies of the AFM and FM from their dispersion relations, Eqs. (10) and (11). For the above parameters, the frequency when the both AFM branches are activated is $f_a = 22.4$ GHz (below f_a the SW propagation is possible only from the “minus” AFM branch). By increasing f to THz range [67], two branches of AFM are converging and SW wavelengths $\lambda_{AFM\pm}$ are decreasing, as shown in Fig. 2(c). In Fig. 2(d) the dependence of T^2 on frequency f is shown without multiplication by ξ (for $\alpha_{ex,2} = 0.3\alpha_{ex,1}$). This leads to $T^2 = 0$ at the activation frequency f_a for the plus AFM branch, and $T^2 = 1$ for the minus AFM branch. The dependence $\xi(f)$ for both AFM branches is shown in the inset of Fig. 2(d).

To control SW propagation via material parameters tuning, it is convenient to consider the dependence of the physical transmittance ξT^2 on frequency. We consider the vicinity of noncompensated case, i.e. when $\mu \ll 1$ [68]. Since for $\alpha_2 > \alpha_1$, the SWs in AFM cannot propagate, we only consider the range $\alpha_2 = [0, \alpha_1]$. The case $\alpha_2 = 0$ is shown in Fig. 3(a), where on the plus AFM branch the physical transmittance in-

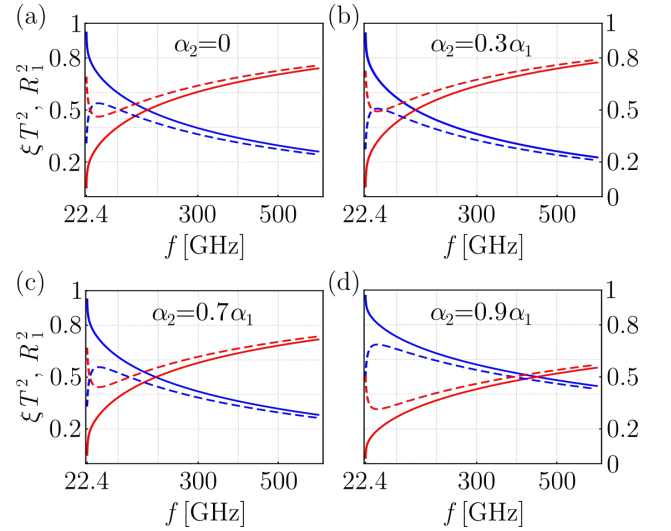


FIG. 3. Normalized transmittance ξT^2 (red solid and dashed lines indicate plus and minus AFM branches, respectively) and reflectance R_1^2 (blue solid and dashed lines indicate plus and minus AFM branches, respectively) as functions of frequency f for four cases: (a) the exchange energy between AFM sublattices at the interface is neglected $\alpha_2 = 0$, (b) $\alpha_2 = 0.3\alpha_1$, (c) $\alpha_2 = 0.7\alpha_1$, and (d) $\alpha_2 = 0.9\alpha_1$.

creases monotonously, while on the minus AFM branch it decreases up to a certain frequency and then increases again. Moreover, at high frequencies the physical transmittances for both AFM branches converge. At very higher frequencies ($\omega \sim 6$ THz), ξT^2 reaches maximum value of 1 and then decreases to zero (and respectively the reflectance reaches minimum value of 0 and then increases at $\omega \rightarrow \infty$ to 1) [69]. Therefore, the full SW reflection or full transmission can be achieved at certain ω . The cases for different α_2/α_1 ratios are shown in Fig. 3(b)-(d). When $\alpha_2 = 0.3\alpha_1$, see Fig. 3(b), for the minus AFM branch, the physical transmittance does not drop below 0.5. Note that at higher frequencies in this range, the physical transmittance is always larger than the reflectance at any α_2 . Meanwhile, to obtain $\xi T^2 > R_1^2$ in a lower-frequency range, it is enough to use the minus AFM branch, as shown in Fig. 3. The phase shifts between the incident and reflected SWs φ_1 and φ_2 are always equal to π , whereas the phase shift between the incident and transmitted SW $\varphi = 0$.

Discussion. Most of the aspects of our SW propagation theory are applicable for any values of the DSNA μ , except for the boundary conditions (2), which are valid only in the vicinity of $\mu = 0$, i.e., for nearly noncompensated AFM/FM interface. Therefore, if one finds the way to generalize these conditions to any μ , the entire theory is immediately extended to any DSNA, thus covering the full range of AFM/FM interfaces: compensated, noncompensated, and anywhere in between. Then our model would also describe AFM/FM interfaces with not only flat profiles, but complex interfaces that take into account surface roughness, diagonal-like interfaces, and even curvilinear interfaces with variable DSNA. Furthermore, an analogous technique may be used to treat the SW

propagation through AFM interfaces with other magnetic media.

Conclusions. We have demonstrated that introducing a new physical characteristic of a finite-thickness interface, the DSNA μ , makes an essential step towards describing a SW propagation through AFM/FM boundary. We have shown that in noncompensated case, by varying the exchange interaction parameter between AFM sublattices, α_2 , fine control of the SW transmittance through the AFM/FM interface can be achieved in the entire range from full reflection to full transmission depending on the SW frequency. This approach may open doors for tailoring interfaces with given AFM exchange constants for future magnonic nanodevices.

Acknowledgments. The authors are grateful to Prof. Yu. Gorobets for very fruitful discussions, who passed away during the preparation of this paper. O.B. and O.G. acknowledge him as a mentor, his guidance and support continue to live on through everyone who knew him. O.B. acknowledges the support of this work by the Academy of Finland (Grants No. 320086 and No. 346035). O.A.T. acknowledges the support by the Australian Research Council (Grant No. DP200101027), the Cooperative Research Project Program at the Research Institute of Electrical Communication, Tohoku University (Japan), and NCMAS grant.

* Oksana.Busel@oulu.fi

† o.tretiakov@unsw.edu.au

- [1] A. H. MacDonald and M. Tsoi, Antiferromagnetic metal spintronics, *Philos. Trans. R. Soc. A* **369**, 3098 (2011).
- [2] A. Chumak, V. Vasyuchka, A. Serga, and B. Hillebrands, Magnon spintronics, *Nat. Phys.* **11**, 453 (2015).
- [3] V. Baltz, A. Manchon, M. Tsoi, T. Moriyama, T. Ono, and Y. Tserkovnyak, Antiferromagnetic spintronics, *Rev. Mod. Phys.* **90**, 015005 (2018).
- [4] Z. Ni, A. V. Haglund, H. Wang, B. Xu, C. Bernhard, D. G. Mandrus, X. Qian, E. J. Mele, C. L. Kane, and L. Wu, Imaging the Néel vector switching in the monolayer antiferromagnet MnPSe₃ with strain-controlled ising order, *Nat. Nanotechnol.* **16**, 782 (2021).
- [5] M. Mohseni, Q. Wang, B. Heinz, M. Kewenig, M. Schneider, F. Kohl, B. Lägel, C. Dubs, A. V. Chumak, and P. Pirro, Controlling the nonlinear relaxation of quantized propagating magnons in nanodevices, *Phys. Rev. Lett.* **126**, 097202 (2021).
- [6] H. Yu, O. d' Allivy Kelly, V. Cros, R. Bernard, P. Bortolotti, A. Anane, F. Brandl, F. Heimbach, and D. Grundler, Approaching soft X-ray wavelengths in nanomagnet-based microwave technology, *Nat. Commun.* **7**, 11255 (2016).
- [7] S. J. Hämäläinen, M. Madami, H. Qin, G. Gubbiotti, and S. van Dijken, Control of spin-wave transmission by a programmable domain wall, *Nat. Commun.* **9**, 4853 (2018).
- [8] C. Liu, J. Chen, T. Liu, F. Heimbach, H. Yu, Y. Xiao, J. Hu, M. Liu, H. Chang, T. Stueckler, S. Tu, Y. Zhang, Y. Zhang, P. Gao, Z. Liao, D. Yu, K. Xia, N. Lei, W. Zhao, and M. Wu, Long-distance propagation of short-wavelength spin waves, *Nat. Commun.* **9**, 738 (2018).
- [9] C. Kim, S. Lee, H.-G. Kim, J.-H. Park, K.-W. Moon, J. Y. Park, J. M. Yuk, K.-J. Lee, B.-G. Park, S. K. Kim, K.-J. Kim, and C. Hwang, Distinct handedness of spin wave across the compensation temperatures of ferrimagnets, *Nat. Mater.* **19**, 980 (2020).
- [10] B. Göbel, I. Mertig, and O. A. Tretiakov, Beyond skyrmions: Review and perspectives of alternative magnetic quasiparticles, *Phys. Rep.* **895**, 1 (2021).
- [11] E. A. Mashkovich, K. A. Grishunin, R. V. Mikhaylovskiy, A. K. Zvezdin, R. V. Pisarev, M. B. Strugatsky, P. C. M. Christianen, T. Rasing, and A. V. Kimel, Terahertz optomagnetism: Non-linear THz excitation of GHz spin waves in antiferromagnetic FeBO₃, *Phys. Rev. Lett.* **123**, 157202 (2019).
- [12] M. Dabrowski, T. Nakano, D. M. Burn, A. Frisk, D. G. Newman, C. Klewe, Q. Li, M. Yang, P. Shafer, E. Arenholz, T. Hesjedal, G. van der Laan, Z. Q. Qiu, and R. J. Hicken, Coherent transfer of spin angular momentum by evanescent spin waves within antiferromagnetic NiO, *Phys. Rev. Lett.* **124**, 217201 (2020).
- [13] J. Cenker, B. Huang, N. Suri, P. Thijssen, A. Miller, T. Song, T. Taniguchi, K. Watanabe, M. A. McGuire, D. Xiao, and X. Xu, Direct observation of two-dimensional magnons in atomically thin CrI₃, *Nat. Phys.* **17**, 20 (2021).
- [14] S. M. Rezende, *Fundamentals of Magnonics*, Vol. 969 (Springer, 2020).
- [15] P. Němec, M. Fiebig, T. Kampfrath, and A. V. Kimel, Antiferromagnetic opto-spintronics, *Nat. Phys.* **14**, 229 (2018).
- [16] X. Zhang, L. Li, D. Weber, J. Goldberger, K. F. Mak, and J. Shan, Gate-tunable spin waves in antiferromagnetic atomic bilayers, *Nat. Mater.* **19**, 838 (2020).
- [17] S. Maendl, I. Stasinopoulos, and D. Grundler, Spin waves with large decay length and few 100 nm wavelengths in thin yttrium iron garnet grown at the wafer scale, *Appl. Phys. Lett.* **111**, 012403 (2017).
- [18] G. Gubbiotti, S. Tacchi, M. Madami, G. Carlotti, A. O. Adeyeye, and M. Kostylev, Brillouin light scattering studies of planar metallic magnonic crystals, *J. Phys. D: Appl. Phys.* **43**, 264003 (2010).
- [19] H. Ulrichs and I. Razdolski, Micromagnetic view on ultrafast magnon generation by femtosecond spin current pulses, *Phys. Rev. B* **98**, 054429 (2018).
- [20] G. Yin, J. X. Yu, Y. Liu, R. K. Lake, J. Zang, and K. L. Wang, Planar Hall Effect in Antiferromagnetic MnTe Thin Films, *Phys. Rev. Lett.* **122**, 106602 (2019).
- [21] J. Železný, H. Gao, K. Výborný, J. Zemen, J. Mašek, A. Manchon, J. Wunderlich, J. Sinova, and T. Jungwirth, Relativistic Néel-order fields induced by electrical current in antiferromagnets, *Phys. Rev. Lett.* **113**, 157201 (2014).
- [22] R. Cheng, J. Xiao, Q. Niu, and A. Brataas, Spin pumping and spin-transfer torques in antiferromagnets, *Phys. Rev. Lett.* **113**, 057601 (2014).
- [23] A. B. Shick, S. Khmelevskiy, O. N. Mryasov, J. Wunderlich, and T. Jungwirth, Spin-orbit coupling induced anisotropy effects in bimetallic antiferromagnets: A route towards antiferromagnetic spintronics, *Phys. Rev. B* **81**, 212409 (2010).
- [24] P. Wadley, K. W. Edmonds, M. R. Shahedkhan, R. P. Champion, B. L. Gallagher, J. Železný, J. Kuneš, V. Novák, T. Jungwirth, V. Saidl, P. Němec, F. Maccherozzi, and S. S. Dhesi, Control of antiferromagnetic spin axis orientation in bilayer Fe/CuMnAs films, *Sci. Rep.* **7**, 11147 (2017).
- [25] L. Shen, J. Xia, X. Zhang, M. Ezawa, O. A. Tretiakov, X. Liu, G. Zhao, and Y. Zhou, Current-induced dynamics and chaos of antiferromagnetic bimerons, *Phys. Rev. Lett.* **124**, 037202 (2020).
- [26] H. Wang, C. Lu, J. Chen, Y. Liu, S. L. Yuan, S. W. Cheong, S. Dong, and J. M. Liu, Giant anisotropic magnetoresistance

- and nonvolatile memory in canted antiferromagnet Sr_2IrO_4 , *Nat. Commun.* **10**, 2280 (2019).
- [27] J. C. Scott, Ferromagnetic resonance studies in the bilayer system $\text{Ni}_{0.80}\text{Fe}_{0.20}/\text{Mn}_{0.50}\text{Fe}_{0.50}$: Exchange anisotropy, *J. Appl. Phys.* **57**, 3681 (1985).
- [28] S. DuttaGupta, A. Kurenkov, O. A. Tretiakov, G. Krishnaswamy, G. Sala, V. Krizakova, F. Maccherozzi, S. S. Dhesi, P. Gambardella, S. Fukami, and H. Ohno, Spin-orbit torque switching of an antiferromagnetic metallic heterostructure, *Nat. Commun.* **11**, 5715 (2020).
- [29] G. M. Mikhailov, A. V. Chernykh, and L. A. Fomin, Application of magnetic force microscopy for investigation of epitaxial ferro- and antiferromagnetic structures, *Materials* **10**, 1156 (2017).
- [30] M. Gruyters and D. Schmitz, Microscopic nature of ferro- and antiferromagnetic interface coupling of uncompensated magnetic moments in exchange bias systems, *Phys. Rev. Lett.* **100**, 077205 (2008).
- [31] V. Puliafito, R. Khymyn, M. Carpentieri, B. Azzerboni, V. Tiberkevich, A. Slavin, and G. Finocchio, Micromagnetic modeling of terahertz oscillations in an antiferromagnetic material driven by the spin Hall effect, *Phys. Rev. B* **99**, 024405 (2019).
- [32] T. Kampfrath, A. Sell, G. Klatt, A. Pashkin, S. Mährlein, T. Dekorsy, M. Wolf, M. Fiebig, A. Leitenstorfer, and R. Huber, Coherent terahertz control of antiferromagnetic spin waves, *Nat. Photonics* **5**, 31 (2011).
- [33] E. G. Tveten, T. Müller, J. Linder, and A. Brataas, Intrinsic magnetization of antiferromagnetic textures, *Phys. Rev. B* **93**, 104408 (2016).
- [34] D. K. Lee, B. G. Park, and K. J. Lee, Antiferromagnetic Oscillators Driven by Spin Currents with Arbitrary Spin Polarization Directions, *Phys. Rev. Appl.* **11**, 054048 (2019).
- [35] L. Shen, J. Xia, G. Zhao, X. Zhang, M. Ezawa, O. A. Tretiakov, X. Liu, and Y. Zhou, Spin torque nano-oscillators based on antiferromagnetic skyrmions, *Appl. Phys. Lett.* **114**, 042402 (2019).
- [36] X. Z. Chen, R. Zarzuela, J. Zhang, C. Song, X. F. Zhou, G. Y. Shi, F. Li, H. A. Zhou, W. J. Jiang, F. Pan, and Y. Tserkovnyak, Antidamping-Torque-Induced Switching in Biaxial Antiferromagnetic Insulators, *Phys. Rev. Lett.* **120**, 207204 (2018).
- [37] T. Shiino, S. H. Oh, P. M. Haney, S. W. Lee, G. Go, B. G. Park, and K. J. Lee, Antiferromagnetic Domain Wall Motion Driven by Spin-Orbit Torques, *Phys. Rev. Lett.* **117**, 087203 (2016).
- [38] L. Baldrati, O. Gomony, A. Ross, M. Filianina, R. Lebrun, R. Ramos, C. Leveille, F. Fuhrmann, T. R. Forrest, F. Maccherozzi, S. Valencia, F. Kronast, E. Saitoh, J. Sinova, and M. Kläui, Mechanism of Néel Order Switching in Antiferromagnetic Thin Films Revealed by Magnetotransport and Direct Imaging, *Phys. Rev. Lett.* **123**, 177201 (2019).
- [39] K. D. Belashchenko, O. Tchernyshyov, A. A. Kovalev, and O. A. Tretiakov, Magnetoelectric domain wall dynamics and its implications for magnetoelectric memory, *Applied Physics Letters* **108**, 132403 (2016).
- [40] T. Moriyama, K. Oda, T. Ohkochi, M. Kimata, and T. Ono, Spin torque control of antiferromagnetic moments in NiO, *Sci. Rep.* **8**, 14167 (2018).
- [41] R. Khymyn, I. Lisenkov, V. S. Tiberkevich, A. N. Slavin, and B. A. Ivanov, Transformation of spin current by antiferromagnetic insulators, *Phys. Rev. B* **93**, 224421 (2016).
- [42] M. Buchner, B. Henne, V. Ney, and A. Ney, Transition from a hysteresis-like to an exchange-bias-like response of an uncompensated antiferromagnet, *Phys. Rev. B* **99**, 064409 (2019).
- [43] O. A. Tretiakov, M. Morini, S. Vasykevych, and V. Slastikov, Engineering curvature-induced anisotropy in thin ferromagnetic films, *Phys. Rev. Lett.* **119**, 077203 (2017).
- [44] X. Xue, Z. Zhou, B. Peng, M. Zhu, Y. Zhang, W. Ren, T. Ren, X. Yang, T. Nan, N. X. Sun, and M. Liu, Electric field induced reversible 180° magnetization switching through tuning of interfacial exchange bias along magnetic easy-axis in multiferroic laminates, *Sci. Rep.* **5**, 16480 (2015).
- [45] B. Li, W. Liu, X. G. Zhao, S. Guo, W. J. Gong, J. N. Feng, T. Yu, and Z. D. Zhang, Modification of exchange bias by cooling field without changing the ferromagnetic magnetization, *J. Magn. Magn. Mater.* **332**, 71 (2013).
- [46] M. Ślęzak, T. Ślęzak, P. Drózdź, B. Matlak, K. Matlak, A. Koziół-Rachwał, M. Zajac, and J. Korecki, How a ferromagnet drives an antiferromagnet in exchange biased CoO/Fe(110) bilayers, *Sci. Rep.* **9**, 889 (2019).
- [47] J. Demeter, E. Menéndez, A. Schrauwen, A. Teichert, R. Steitz, S. Vandezande, A. R. Wildes, W. Vandervorst, K. Temst, and A. Vantomme, Exchange bias induced by O ion implantation in ferromagnetic thin films, *J. Phys. D: Appl. Phys.* **45**, 405004 (2012).
- [48] V. V. Kruglyak, O. Y. Gorobets, Y. I. Gorobets, and A. N. Kuchko, Magnetization boundary conditions at a ferromagnetic interface of finite thickness, *J. Phys. Condens. Matter* **26**, 406001 (2014).
- [49] J. F. Cochran and B. Heinrich, Boundary conditions for exchange-coupled magnetic slabs, *Phys. Rev. B* **45**, 13096 (1992).
- [50] J. W. Klos, Y. S. Dadoenkova, J. Rychly, N. N. Dadoenkova, I. L. Lyubchanskii, and J. Barnaś, Hartman effect for spin waves in exchange regime, *Sci. Rep.* **8**, 17944 (2018).
- [51] The dissipation generally decreases the amplitudes of SWs, but does not influence their behavior qualitatively. Therefore, in the following we can use the LL equation approximation, where the dissipation is neglected.
- [52] V. G. Bar'yakhtar, B. A. Ivanov, and M. V. Chetkin, Dynamics of domain walls in weak ferromagnets, *Sov. Phys. Usp.* **28**, 563 (1985).
- [53] V. Bar'yakhtar, B. Ivanov, and A. Sukstanskii, Nonlinear waves and the dynamics of domain walls in weak ferromagnets, *Sov. Phys. JETP* **51**, 757 (1980).
- [54] E. G. Tveten, A. Qaiumzadeh, O. A. Tretiakov, and A. Brataas, Staggered dynamics in antiferromagnets by collective coordinates, *Phys. Rev. Lett.* **110**, 127208 (2013).
- [55] J. Barnas, On the Hoffmann boundary conditions at the interface between two ferromagnets, *J. Magn. Magn. Mater.* **102**, 319 (1991).
- [56] O. Busel, O. Gorobets, and Y. Gorobets, Boundary conditions at the interface of finite thickness between ferromagnetic and antiferromagnetic materials, *J. Magn. Magn. Mater.* **462**, 226 (2018).
- [57] O. Busel, O. Gorobets, and Y. Gorobets, Propagation of Spin Waves Through an Interface Between Ferromagnetic and Antiferromagnetic Materials, *J. Supercond. Nov. Magn.* **32**, 3097 (2019).
- [58] See Sec. I of the Supplemental Material [59].
- [59] See supplemental material at [url will be inserted by publisher] for additional information.
- [60] See Sec. II of the Supplemental Material [59].
- [61] We consider the interface as a composite material that includes three magnetizations - two from AFM sublattices and one from FM, as shown in Fig. (1). However, according to [48] for finding the boundary conditions in the form of Eqs. (2), the only case when magnetization of one of AFM sublattices is parallel and comparable in magnitude to the FM magnetization is

- appropriate, i.e., noncompensated AFM boundary case $\mu \rightarrow 0$.
- [62] A. I. Akhiezer, V. G. Bar'yakhtar, and S. V. Peletminskii, *Spin Waves* (North-Holland, Amsterdam, 1968).
- [63] In realistic systems, the energy is lost at the boundary, however, generally this loss would not effect qualitatively the results of the proposed model if taken into account.
- [64] For the derivation of ξ see Sec. IV of the Supplemental Material [59].
- [65] See Sec. IV of the Supplemental Material [59].
- [66] E. G. Tveten, A. Qaiumzadeh, and A. Brataas, Antiferromagnetic domain wall motion induced by spin waves, *Phys. Rev. Lett.* **112**, 147204 (2014).
- [67] Note that at very high frequencies the LL equation stops being applicable and our description is not valid anymore.
- [68] Despite the fact that the magnitudes of the magnetization in FM and sublattice magnetization in the AFM have to be approximately equal, i.e. $\nu \approx 1$, we have tested the limits of our model applicability for various values of ν within the range [0.5, 1.5], thus confirming that it only leads to quantitative variations.
- [69] See Sec. V of the Supplemental Material [59].